Journal of Inflammation Research

Dovepress
Taylor & Francis Group

Open Access Full Text Article

ORIGINAL RESEARCH

Maxing Shigan Decoction Alleviates Lung Heat Syndrome by Inhibiting α4β7-Mediated γδT17 Cell Migration Across the Gut-Lung-Nasal Axis

Jingyi Zhao, Junge Wang, Xinyu Yan, Suying Guo, Man Wang

Department of Otolaryngology, Beijing Hospital of Traditional Chinese Medicine, Beijing, People's Republic of China

Correspondence: Junge Wang, Email wangjunge@bjzhongyi.com

Purpose: Lung Heat Syndrome (LHS), a pathological state in Traditional Chinese Medicine characterized by pulmonary inflammation, lacks mechanistic understanding of its gut-lung-nasal axis involvement. Maxing Shigan decoction (MXSGD) clinically resolves LHS, but its immunomodulatory mechanisms remain unclear. This study aimed to elucidate the specific immunomodulatory mechanism through which MXSGD alleviates LHS, focusing on its role in regulating γδT17 cell migration along the gut-lung-nasal axis via the α4β7 pathway.

Methods: Network pharmacology and molecular docking identified MXSGD's bioactive components and targets. Mice were randomized into Control, LHS, and different doses of MXSGD groups. LHS was induced by cold stress with intratracheal lipopolysaccharide, and MXSGD was administered orally. Water intake, respiratory rate, and locomotor activity were monitored. CFSE-labeled γδT17 cells were adoptively transferred. CCL25 levels were manipulated using recombinant protein or neutralizing antibody, and α4β7 integrin was blocked with specific antibody. Tissues were analyzed by H&E staining, flow cytometry, ELISA and RT-PCR.

Results: Network pharmacology analysis identified 142 shared targets between MXSGD and LHS, with significant enrichment in interleukin-17A (IL-17A) and T cell receptor signaling pathways. MXSGD significantly alleviated reduced water intake and attenuated neutrophil infiltration in ileum and lung. MXSGD inhibited γδT17 cell migration in the lungs and nose, while downregulating IL-17A production in the ileum and lungs and RORγt expression across all tissues. Recombinant CCL25 increased the frequencies of γδT17 cells in the ileum and lungs and $\alpha4\beta7^{+}$γδT17 cells in the lungs, and elevated IL-17A levels in all tissues. These effects were reversed by CCL25 neutralization. α4β7 blockade inhibited γδT17 recruitment and IL-17A production in nose.

Conclusion: MXSGD alleviated LHS by inhibiting CCL25/α4β7-dependent γδT17 cell migration and IL-17 production. The study demonstrated γδT17 trafficking as the cellular basis for gut-lung-nasal axis interaction in LHS, while positioning MXSGD as a promising therapy for IL-17-driven respiratory inflammation.

Keywords: maxing Shigan decoction, lung heat syndrome, γδT17 cells, gut-lung-nasal axis, C-C motif chemokine 25, α4β7 integrin

Introduction

"Lung Heat Syndrome" (LHS) is a common diagnostic concept in Traditional Chinese Medicine (TCM), describing a pathological state characterized by excessive heat in the lungs. The heat can arise from infections, wind-cold invasion, or internal imbalances caused by emotional stress or dietary habits. "Lung Heat Syndrome" can be likened to inflammatory processes such as sore throat, cough, thick yellow sputum, or nasal dryness in acute bronchitis, pneumonia, and other respiratory diseases.[1–5] Maxing Shigan Decoction (MXSGD), a classical formula in TCM, has been widely used for centuries to treat LHS through its unique multi-target compositional strategy.

As the monarch herb, *Ephedra sinica Stapf* (Chinese name: "Ma huang", MH) opens the lung Qi to relieve wheezing and disperses "wind-cold" pathogens from the exterior. Meanwhile, *Gypsum fibrosum* (Chinese name: "Sheng shi gao", SSG), the minister herb, clears lung and stomach "heat" to resolve interior fire. This "exterior-interior" duality is further

Received: 2 August 2025
Accepted: 15 November 2025
Published: 26 November 2025

Graphical Abstract

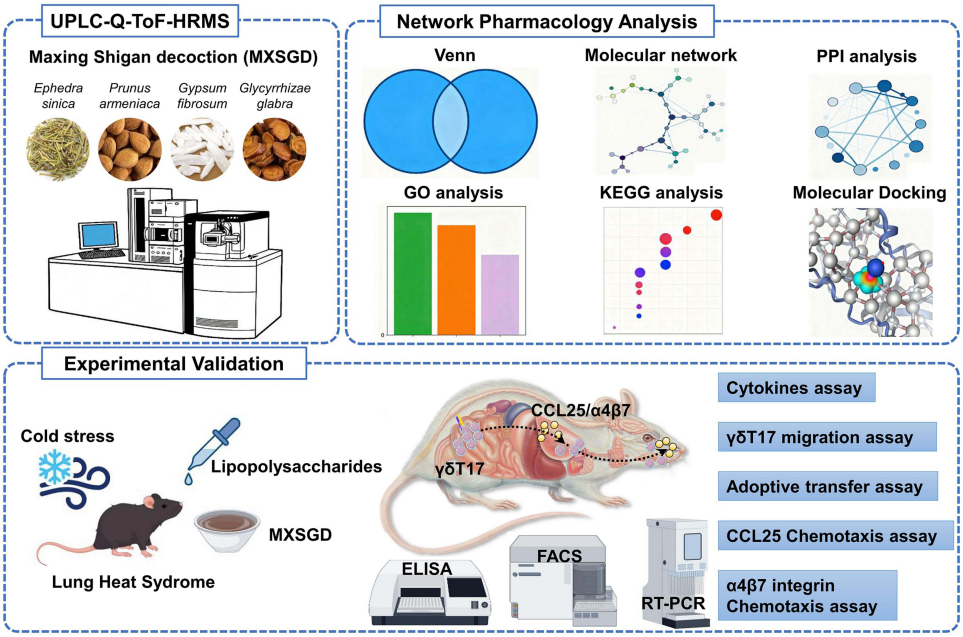

supported by *P Prunus armeniaca L*. (Chinese name: "Ku xing ren", KXR), which directs lung Qi downward to suppress cough, and *Glycyrrhizae glabra L*. (Chinese name: "Zhi gan cao", ZGC), which harmonizes the formula while potentiating anti-inflammatory effects. Modern pharmacological studies have elucidated the mechanisms of its action, including anti-inflammatory, antiviral, and immunomodulatory effects.[6–9] The formula exerts a dual-action mechanism of "releasing the exterior and clearing the interior",[10] making it uniquely effective in addressing both superficial and deep-seated pathological factors.

LHS may be intricately associated with intestinal and nasal compartments through immune-mediated pathways.[11,12] TCM holds that excessive heat in lung disrupts intestinal motility and leading to constipation or diarrhea through meridians. As the orifice of the lung, the nasal cavity serves as a direct conduit for heat expulsion. Emerging evidence demonstrated that mucosal immunity interconnects nasal, pulmonary, and intestinal inflammatory responses via T helper 17 cell (Th17)- and interleukin-17 (IL-17)-driven cytokine axes.[13–16] Nevertheless, the specific cellular mediators and chemotactic signals orchestrating this crosstalk in LHS remain poorly characterized.

γδT17 cells represent a unique subset of γδT lymphocytes that found predominantly in mucosal tissues and barrier surfaces, especially in gut, where they contribute to immune surveillance and pathogen clearance.[17,18] Once activated, γδT17 cells secrete cytokine IL-17A to amplify inflammatory responses.[19] The migration of γδT cells to specific tissues is tightly regulated by C-C motif chemokine ligand 25 (CCL25), which is predominantly expressed by epithelial cells in the small intestine.[20] CCL25 is crucial for T-cell development in the thymus, where it facilitates the migration of immature T-cells through the thymic cortex and medulla.[21] α4β7 integrin is a heterodimeric receptor that expressed on T cells, binds to mucosal addressin cell adhesion molecule-1 on endothelial cells, facilitating the migration of lymphocytes to the mucosal barrier.[22] Studies have shown that γδT cells expressing α4β7 are preferentially localized in the intestinal epithelium, where they interact with epithelial cells and contribute to the regulation of immune responses.[23,24] However, the precise immunomodulatory pathways linking MXSGD to mucosal immune regulation across the gut-lung-nasal axis remain poorly understood, particularly in the context of γδT17 cell dynamics.

In this study, we employed integrated network pharmacology, molecular docking, and in vivo approaches to investigate MXSGD's immunomodulatory mechanism in a murine LHS model. We demonstrate that MXSGD alleviated pathological symptoms and mucosal inflammation by specifically suppressing CCL25 and α4β7 integrin dependent migration of γδT17 cells across the gut-lung-nasal axis. Our results reveal γδT17 cell trafficking as the cellular basis for axis crosstalk in LHS and identify MXSGD's bioactive components as inhibitors of α4β7-mediated homing.

Materials and Methods

Plant Materials and Main Reagents

All herbs were ordered from Beijing Chunfeng Pharmaceutical (Beijing, China) through Beijing Hospital of Traditional Chinese Medicine. A voucher specimen was deposited at the Herbarium of Beijing College of Traditional Chinese Medicine (Code: BCMM). Reference standards ephedrine (171237–202106), pseudoephedrine (171241–202003), amygdalin (110820–202201), liquiritin (111610–202007) and glycyrrhizic acid (110731–202111) were obtained from National Institutes for Food and Drug Control.

Analytical-grade methanol (A456-4), acetonitrile (A955-4), formic acid (A117-50), anti-mouse IL-17A antibody (17–7177-82), mouse IL-17 ELISA Kit (BMS6001), and mouse CCL25 ELISA Kit (EMCCL25X10) were purchased from Thermo Fisher Scientific (Shanghai, China). Anti-Mouse TCR γ/δ Antibody (118108), brefeldin A (420601), PE anti-mouse Integrin α4β7 Antibody (120605), and Recombinant Mouse CCL25 Protein (577402) were obtained from BioLegend (San Diego, CA, USA). Anti-Mouse CD3 Antibody (553066) was purchased from BD Biosciences (Franklin Lakes, NJ, USA). Phorbol 12-myristate 13-acetate (P8139), ionomycin (I9657), and protease inhibitor cocktail (P8340) were purchased from Sigma-Aldrich (St. Louis, MO, USA). QuantiTect SYBR Green RT-PCR Kit (204243) was purchased from QIAGEN (Shanghai, China).

Preparation of MXSGD

The ratio of the four herbs (*E. sinica, P. armeniaca, G. fibrosum*, and *G. glabra*) in MXSGD was 2:2:4:1. The four ingredients were prepared according to the method described in previous study,[20] briefly first decoction of *E. sinica* in 1000mL of distilled water for 10 minutes, followed by sequential addition of the remaining botanical specimens and extended thermal extraction for 20 min. The extraction was then filtered through sterile gauze and concentrated using a rotavapor at a final concentration of 1.40 g/mL and stored at 4°C. The main components of the MXSGD decoction were analyzed using Ultra-Performance Liquid Chromatography Quadrupole-Time-of-Flight Mass Spectrometry (UPLC-Q-ToF-HRMS).

Network Pharmacological Analysis and Molecular Docking

Collection of Active Components and Targets In MXSGD

The collection of active components and their targets in MXSGD were retrieved from the Traditional Chinese Medicine Systems Pharmacology Database and Analysis Platform (https://www.tcmsp-e.com/tcmsp.php). Comprehensive analysis was performed on herbal components Ephedra sinica, Prunus Armeniaca, and Glycyrrhizae glabra. Active components were screened based on the recommended criteria of oral bioavailability ≥30% and drug-likeness ≥0.18. Gypsum Fibrosum was identified as "calcium sulfate dihydrate" in the PubChem Database (https://pubchem.ncbi.nlm.nih.gov/). Functional annotation of the active components was collected through the UniProt Database (https://www.uniprot.org/), where only reviewed targets were selected.

Collection of Targets Between MXSGD and LHS

To elucidate the molecular mechanisms of MXSGD in the treatment of LHS, analysis of shared targets was conducted. Initially, "pharyngalgia", "cough", and "phlegm" were identified as representative symptoms of LHS, and associated targets were screened from the GeneCards Database (https://www.genecards.org/) and OMIM Database (https://omim.org/). The intersection of targets was identified using the bioinformatics tool jvenn[25] (http://www.bioinformatics.com.cn/static/others/

jvenn/example.html). To further characterize the molecular network, Cytoscape 3.10.1 was employed to construct a network model linking the herbal components of MXSGD, active ingredients, and the shared targets with LHS.

Protein-Protein Interaction (PPI) Enrichment Analysis

PPI enrichment analysis was performed using the Metascape platform (http://metascape.org/gp/index.html) to analyze the network of overlapping genes between MXSGD and LHS. The Molecular Complex Detection (MCODE) algorithm was subsequently applied to identify densely connected network components, which were further subjected to independent pathway and process enrichment analysis to elucidate their functional roles and biological significance.

GO and KEGG Pathway Analysis

Gene Ontology (GO) and Kyoto Encyclopedia of Genes and Genomes (KEGG) pathway analyses were performed using the DAVID database (https://davidbioinformatics.nih.gov/) to investigate the shared targets between MXSGD and LHS, and significant terms with a Benjamini-Hochberg adjusted p-value < 0.05 were selected. The enrichment analysis was performed using the whole genome as the background gene set. The results were visualized using the SRplot tool[26] (http://bioinformatics.com.cn/srplot).

Molecular Docking

The binding energy and interaction mode between MXSGD and α4β7 integrin were assessed through molecular docking analysis. The structural coordinates of α4β7 integrin (PDB ID: 3V4P) were obtained from the RCSB Protein Data Bank (https://www.rcsb.org/). Preprocessing of the target protein was conducted using PyMol 4.6.0, including the removal of water molecules and polar hydrogen atoms. The chemical structures of the nine compounds in MXSGD confirmed via UPLC-Q-ToF-HRMS were retrieved from the PubChem database. Molecular docking studies were implemented using AutoDock 1.5.7. The binding pocket was defined with coordinates (−0.79, 33.95, 17.27) and a grid box of dimensions (40×40×40) Å. The binding affinity and interaction mode were analyzed based on the calculated binding energy values. Visualizations of the protein-ligand interactions were created using PyMol.

Animals

Twenty-four female C57BL/6 mice, aged 6–8 weeks (weighing approximately 18 to 22 g each), were purchased from Charles River Laboratories Animal Technology Co., Ltd. (Beijing, China). The mice were acclimatized to the new environment for 1 week. The adopted diet was provided *ad libitum*, with free access to water and standard chow, comprising 54% mixed carbohydrate, 19% protein and 3% lipid by weight, and was maintained under conditions with a temperature of 18–20°C, humidity of 40–60% and a light/dark cycle of 12 h. All efforts were made to ameliorate the welfare and to minimize animal suffering.

The mice were randomly assigned to three groups (8 per group) using a computer-generated random sequence as follows: (1) naive group (Control); (2) LHS group; (3) MXSGD-H and MXSGD-L group, LHS mice treated with MXSGD, 7.02 mg/g according to the conversion by body surface area.

Induction of LHS

Mice in the LHS group were placed in a temperature-regulated chamber for 3 consecutive days under controlled environmental conditions (temperature: 10°C, humidity: 50–55%, wind speed: 2 m/s) for 4 hours daily to induce exposure to wind-cold pathogens. On days 5 and 12 post-modeling, mice were anesthetized via intraperitoneal injection of 1% sodium pentobarbital, followed by intratracheal administration of 0.1 mL lipopolysaccharide (LPS, 1 mg/mL). Mice in the MXSGD-H and MXSGD-L groups received daily oral gavage, 14.04 mg/g and 7.02 mg/g respectively, from days 19 to 25. In parallel, the LHS group was administered an equivalent volume of phosphate-buffered saline (PBS). The control group received both intratracheal PBS instillation and oral PBS gavage as a baseline comparison (Figure 1). Open-field test was performed to assess locomotor activity in mice. Each mouse was placed in the center of a square arena (40 × 40 × 30 cm) under dim illumination (50 lux), and its movement was recorded for 5 minutes using an automated tracking system (EthoVision XT). Total distance traveled was quantified at days 1, 2, 3, 4, 5, 12, 18, and 25

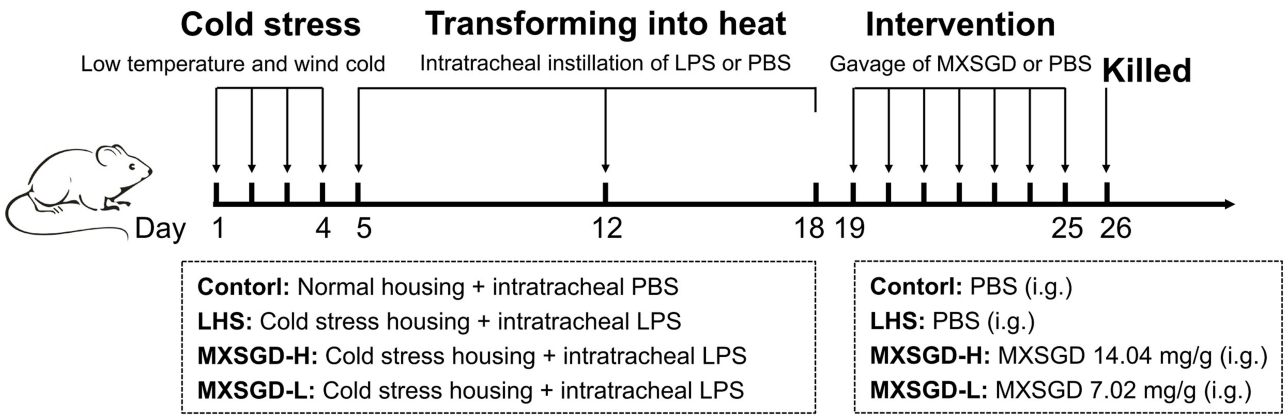

Figure 1 Modeling flow chart.

post-modeling to evaluate longitudinal changes in exploratory behavior. Twenty-four hours after the final gavage, all mice were anesthetized with pentobarbital and euthanized for tissue collection.

Histopathological Analysis

For histopathological examination, tissue samples from the ileum, lung, and nasal mucosa were collected. The samples were fixed in 10% neutral buffered formalin for 24 hours, followed by dehydration through graded ethanol and embedded in paraffin wax. 5 μm thick sections were cut and subjected to hematoxylin and eosin (H&E) staining. Histological changes were examined under a light microscope and captured for analysis.

Flow Cytometry Assay

To quantify the percentage of γδT17 cells in the ileum, lung, and nasal mucosa, flow cytometry was performed as follows. Tissues were dissected and placed in a Petri dish, enzymatically digested, filtered through a 70-μm cell strainer, and centrifuged at 300 × g for 5 minutes at 4°C. The cell pellet was resuspended in PBS, and the mononuclear cell layer was collected after density gradient centrifugation. Cell concentrations were adjusted to 1.0×10^6 cells per tube in complete RPMI-1640 medium. For γδT17 cell detection, cells were stimulated with phorbol 12-myristate 13-acetate (PMA, 50 ng/mL), ionomycin (1 μg/mL), and brefeldin A (5 μg/mL) at 37°C in a 5% CO_2 incubator for 4 hours. Subsequently, cells were stained with anti-CD3 (0.25 μg/test), anti-TCRγ/δ (2 μg/test), anti-α4β7 integrin (2.5 μg/test) antibodies or corresponding isotype controls at 4°C for 30 minutes, followed by fixation and permeabilization. Intracellular staining was performed using anti-IL-17A antibody (1 μg/test) at 4°C for 30 minutes. Cells were then washed twice with PBS, resuspended, and analyzed using a BD FACSVerse flow cytometer (BD Biosciences, Franklin Lakes, NJ, USA). Data were analyzed with FlowJo software version 10.0 (BD Biosciences, Franklin Lakes, NJ, USA).

Enzyme-Linked Immunosorbent Assay

The ileum, lung, and nasal mucosa were homogenized in ice-cold PBS containing a protease inhibitor cocktail. The homogenates were centrifuged at 10,000 × g for 15 minutes at 4°C, and the supernatants were collected. IL-17A, IL-1β, IL-23 and CCL25 levels were measured using the ELISA kit according to the manufacturer's instructions. The concentrations were calculated based on the standard curve.

Reverse Transcription-Polymerase Chain Reaction Assay

The ileum, lung, and nasal mucosa were cut into approximately 2 mm^3 pieces under liquid nitrogen and homogenized. First-strand cDNA was synthesized from 1 μg of total RNA according to the manufacturer's instructions. RT-PCR was performed using SYBR Green Master Mix on a real-time PCR system. The reaction conditions were set as initial denaturation at 95°C for 10 minutes, followed by 40 cycles of denaturation at 95°C for 15 seconds, annealing at 60°C for 30 seconds, and extension at

72°C for 30 seconds. The primer sequences were as follows: β-actin (forward: 5′-GCAGGAGCAATGGAAGTCG-3′, reverse: 5′-CGCTGAGGAAGTGGGAAAA-3′), RORγt (forward: 5′-TAAAGACCTCTATGCCAACACAGT-3′, reverse: 5′-CACGATGGAGGGCCCGGACTCATC-3′). The relative expression of RORγt was calculated using the $2^{-\Delta\Delta Ct}$.

Adoptive Transfer Assay

Intestinal γδT17 cells were isolated from the ileum of normal C57BL/6 mice (n=5) following anesthesia. Tissues were digested, filtered, and centrifuged to obtain mononuclear cells, and enriched for γδT cells using a TCRγ/δ$^+$ T cell isolation kit. The purified γδT cells were further stained with PE-labeled IL-17A antibody and anti-PE microbeads, achieving a purity of >90% as confirmed by flow cytometry. For cell tracking, γδT17 cells were labeled with carboxy fluorescein succinimidyl ester (CFSE) according to the manufacturer's protocol. CFSE$^+$ γδT17 cells (1×10^5) were then intravenously injected into mice 24 hours prior to the induction of LHS. The distribution of CFSE$^+$ γδT17 cells in the ileum, lung, and nasal mucosa was quantified using flow cytometry.

Chemotaxis Assay

Twenty-four C57BL/6 mice were randomly divided into high-CCL25 (CCL25-H), low-CCL25 (CCL25-L), and control groups. The CCL25-H group received intravenous injections of 0.2 mL recombinant mouse CCL25 (rmCCL25, 1 μg/mL) via tail vein 1 hour before wind-cold exposure. The CCL25-L group was injected with 0.2 mL of CCL25-neutralizing antibody (0.5 mg/mL), while the control group received PBS. Flow cytometry was used to quantify γδT17 cells and α4β7$^+$γδT17 subsets. IL-17A levels was measured with the ELISA kit.

Sixteen C57BL/6 mice were randomly assigned to α4β7-blocked group and control group. The α4β7-blocked group received intravenous injections of 0.2 mL of monoclonal α4β7 antibody (0.5 mg/mL) 1 hour before wind-cold exposure, while the control group received PBS. All other procedures were consistent with those used in the MXSGD group. Flow cytometry was used to quantify γδT17 cells subsets. IL-17A and CCL25 levels was measured with the ELISA kit.

Statistical Analysis

Statistical analyses were performed using GraphPad Prism 10.4.1 (GraphPad Software, La Jolla, CA, USA). Data were tested for normality and equal variance prior to analysis. Comparisons between two groups were performed using an unpaired two-tailed *t*-test. Comparisons among more than two groups were conducted using one-way analysis of variance followed by Tukey's post hoc test for pairwise comparisons. A p-value of less than 0.05 ($P < 0.05$) was considered statistically significant.

Results

UPLC-Q-ToF-HRMS Analysis

In the present study, UPLC-Q-ToF-HRMS analysis of MXSGD was conducted in both positive and negative ion modes. A total of 114 chemical constituents were identified (Supplementary Table 1), among which amygdalin, ephedrine, glycyrrhizic acid, L-epicatechin, liquiritin, methylephedrine, procyanidin B1, rutin, and stachydrine were characterized as the predominant bioactive components (Figure 2). These findings align with prior report[27] on MXSGD's herbal constituents, wherein ephedrine derivatives and glycoside compounds were highlighted as key contributors to the pharmacological activity.

Network Pharmacology Analysis of MXSGD in Treating LHS

The active components of MXSGD involved in the treatment of LHS were identified using the TCMSP database, which identified three herbs (*E. sinica, P. armeniaca*, and *G. glabra*) containing 162 chemicals and a total of 228 potential targets. The 12 potential targets of *F. gypsum* were identified via the UniProt database. LHS-related targets were retrieved from the GeneCards and OMIM databases, resulting in the identification of 2,130 genes. Overlapping genes were calculated and visualized using the jVenn online tool, revealing 142 overlapping target genes associated with both MXSGD and LHS (Figure 3). These genes were subjected to functional enrichment analysis using the Metascape to

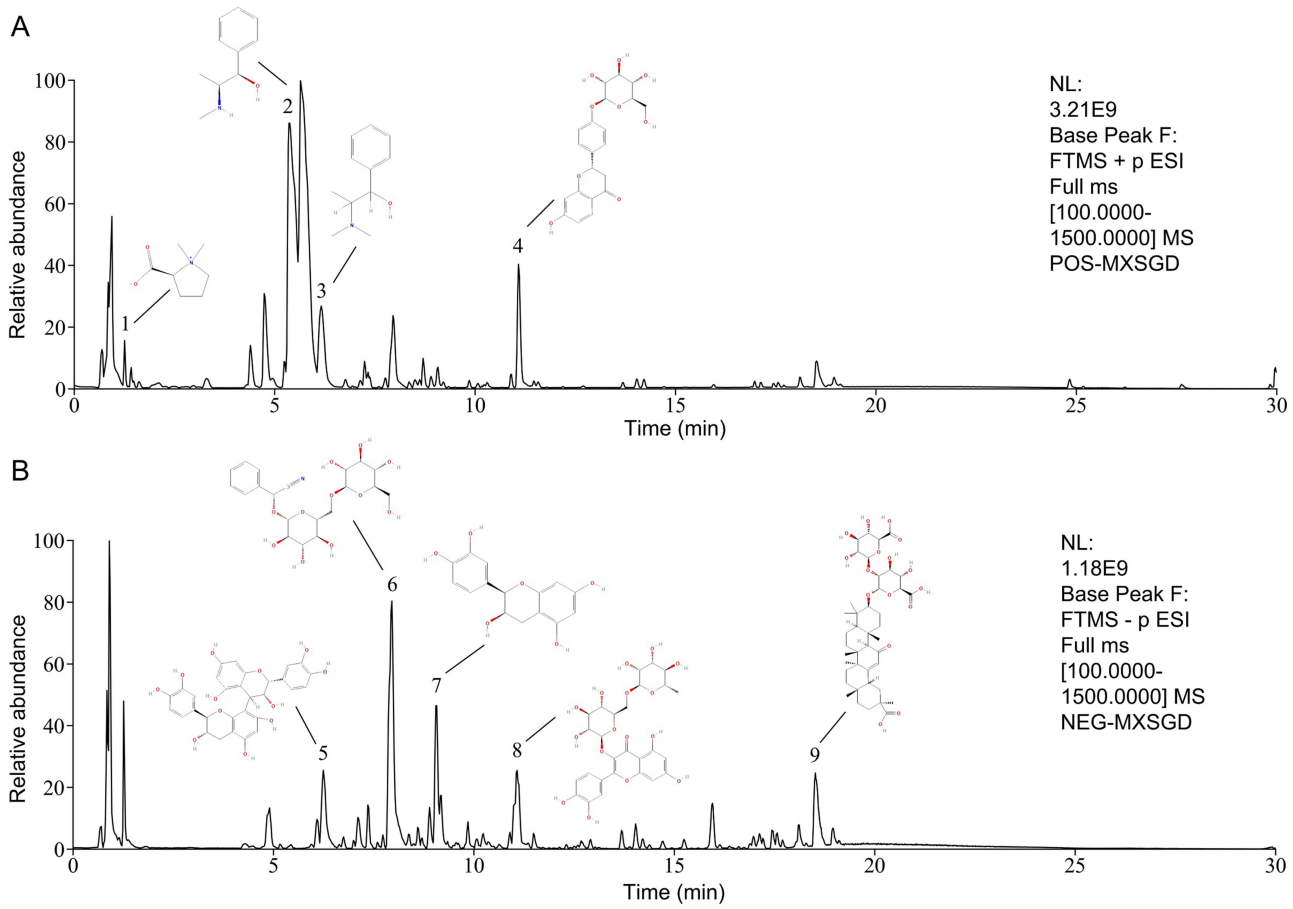

Figure 2 Total ion chromatograms of MXSGD extract via UPLC-Q-TOF-MS. (**A**) Positive ion mode. (**B**) Negative ion mode. 1- stachydrine, 2- ephedrine, 3-methylephedrine, 4- liquiritin, 5- procyanidin B1, 6- amygdalin, 7- L-epicatechin, 8- rutin, 9- glycyrrhizic acid.

identify potential pathways. As illustrated in Figure 3B, PPI analysis revealed 8 gene clusters. A visualization network was constructed to depict the relationships between the four herbs, their active components, and the overlapping genes associated with LHS (Figure 3). This network highlighted quercetin as the most significant active component in MXSGD for treating LHS.

To further identify potential pathways associated with MXSGD in treating LHS, GO and KEGG enrichment analyses were performed using the DAVID bioinformatics platform. GO analysis identified 348 significantly enriched terms ($P < 0.05$), categorized into biological processes (BP, 97 terms, 28%), cellular components (CC, 83 terms, 24%), and molecular functions (MF, 168 terms, 48%) (Figure 3). Enriched BP terms were predominantly associated with inflammatory response and positive regulation of cell population proliferation, while MF terms highlighted enzyme binding and protein kinase activity. KEGG analysis revealed 162 significant signaling pathways ($P < 0.05$), including IL-17 signaling pathway and the T cell receptor signaling pathway. Both pathways are closely associated with γδT cell-mediated inflammation (Figure 3).

Molecular Docking of Major Components of MXSGD with α4β7 Integrin

Molecular docking studies were performed to investigate the binding affinity of eight major components identified via UPLC-Q-ToF-HRMS in MXSGD with the α4β7 integrin. The binding affinity of the compounds was evaluated based on their calculated binding energy values (Table 1). The binding energy values indicate that glycyrrhizic acid (ΔG = −11.547 kcal/mol) and liquiritin (ΔG = −13.676 kcal/mol) exhibited the strongest binding affinities to α4β7 integrin. The visualization of protein-ligand interactions revealed key hydrogen bonding and hydrophobic interactions that stabilized the binding of these compounds to α4β7 integrin (Figure 4).

https://doi.org/10.2147/JIR.S557792

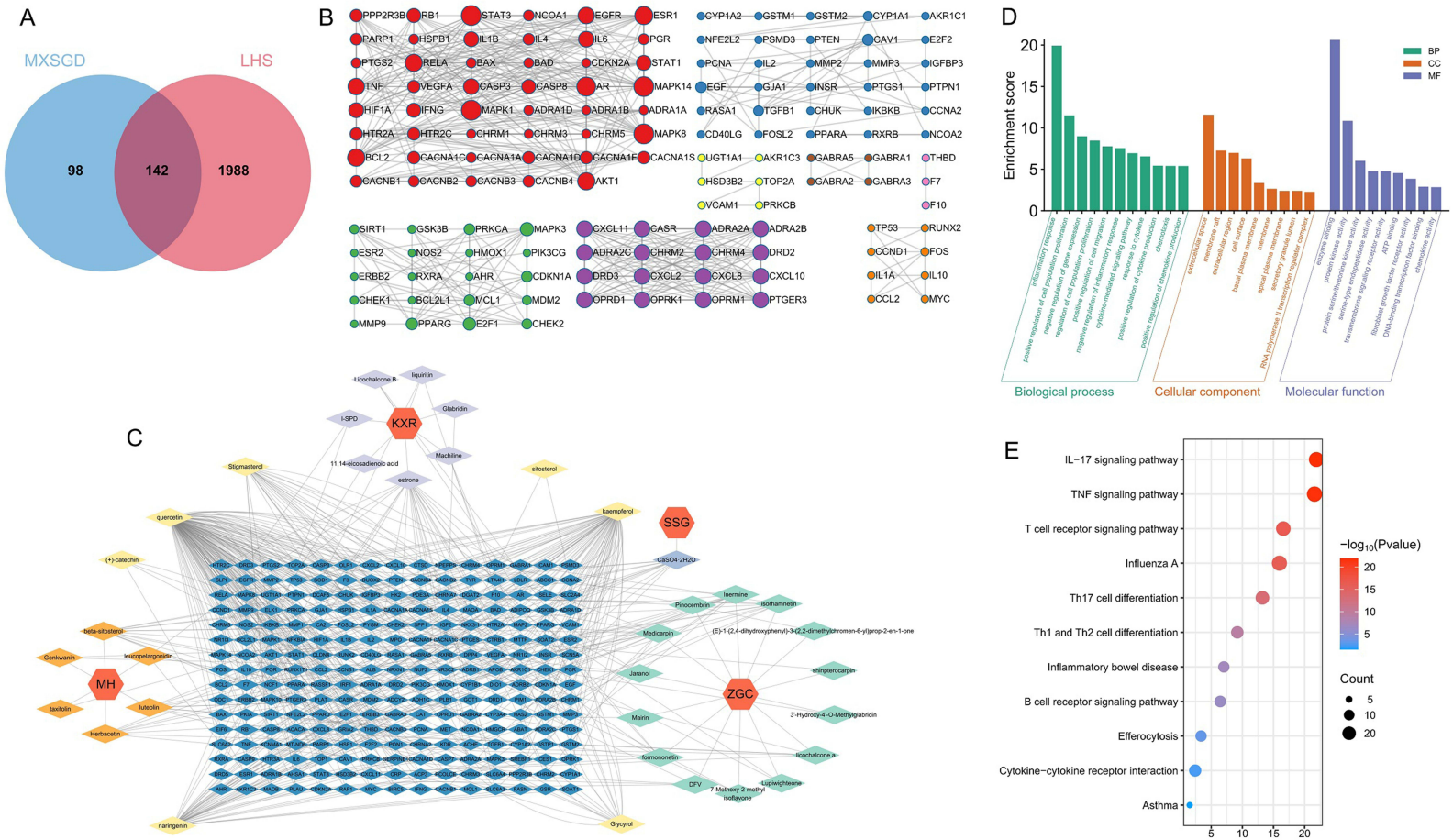

Figure 3 Network pharmacology analysis of MXSGD for LHS treatment. (**A**) Venn diagram of overlapping targets between MXSGD and LHS. (**B**) Protein-protein interaction enrichment analysis of 142 overlapping genes using Metascape. (**C**) Network diagram of MXSGD herbs, active components, and targets with LHS. (**D**) GO functional enrichment analysis. (**E**) KEGG pathway enrichment analysis.

Table 1 Binding Energy Values of MXSGD Components with α4β7 Integrin

Compound	Binding Energy (kcal/mol)
Liquiritin	−13.676
Glycyrrhizic acid	−11.547
Procyanidin B1	−11.508
Ephedrine	−10.517
Methylephedrine	−9.325
Stachydrine	−8.159
Amygdalin	−7.873
Rutin	−6.024
L-Epicatechin	−4.65

Effects of MXSGD on Physiological Parameters and Inflammatory Responses

Water intake, respiratory rate and locomotor activity were monitored in C57BL/6 mice on days 1, 2, 3, 4, 5, 12, 18, and 25. The LHS group showed progressively increased water intake following LPS challenges, peaking at 44.95 mL on day 25; this polydipsia was attenuated by MXSGD administration, with MXSGD-H (32.6–38.66 mL) and MXSGD-L (33.3–41.1 mL) maintaining lower intake than LHS during intervention (Figure 5). Respiratory rates remained stable initially (Control: 111–147 breaths/min; LHS: 90–130 breaths/min), but LHS exhibited a pronounced increase post-LPS challenge (day 5), persisting on days 12 and 18; MXSGD intervention from day 19 modulated this response, reducing rates in MXSGD-H and MXSGD-L groups relative to LHS by day 25 (Figure 5). Locomotor activity analysis revealed persistently reduced total distance in LHS versus controls throughout the 25-day period, though MXSGD-H approached control levels by day 18 and MXSGD-L showed partial recovery. Transient hyperactivity occurred in all groups on day 5, indicating LHS impaired exploratory drive while

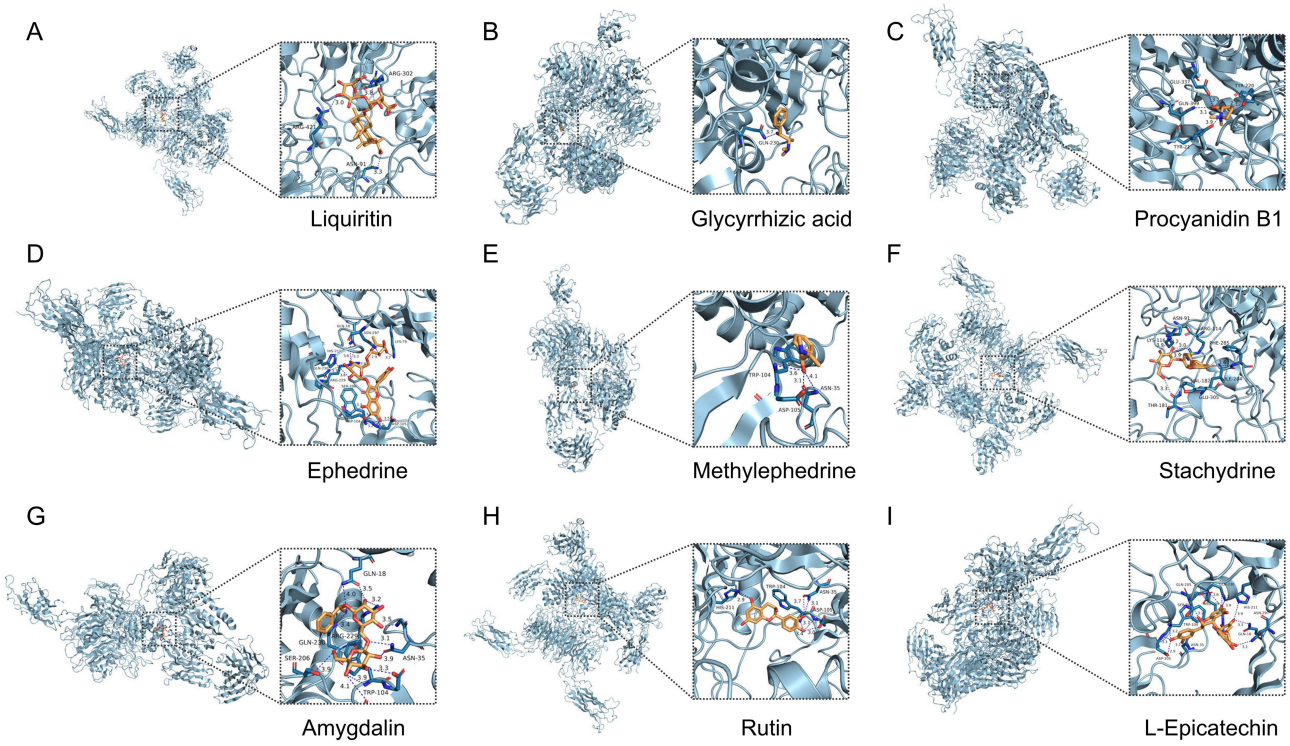

Figure 4 Molecular docking of α4β7 integrin with small molecules in MXSGD. Molecular docking results of α4β7 integrin with eight small molecules identified in MXSGD. (**A**) Liquiritin. (**B**) Glycyrrhizic acid. (**C**) Procyanidin B1. (**D**) Ephedrine. (**E**) Methylephedrine. (**F**) Stachydrine. (**G**) Amygdalin. (**H**) Rutin. (**I**) L-Epicatechin. Each panel corresponds to one small molecule and displays the name and structure, cartoon format of the docking result, close-up view of the binding region. Hydrogen bonds are represented by dashed yellow lines.

https://doi.org/10.2147/JIR.S557792

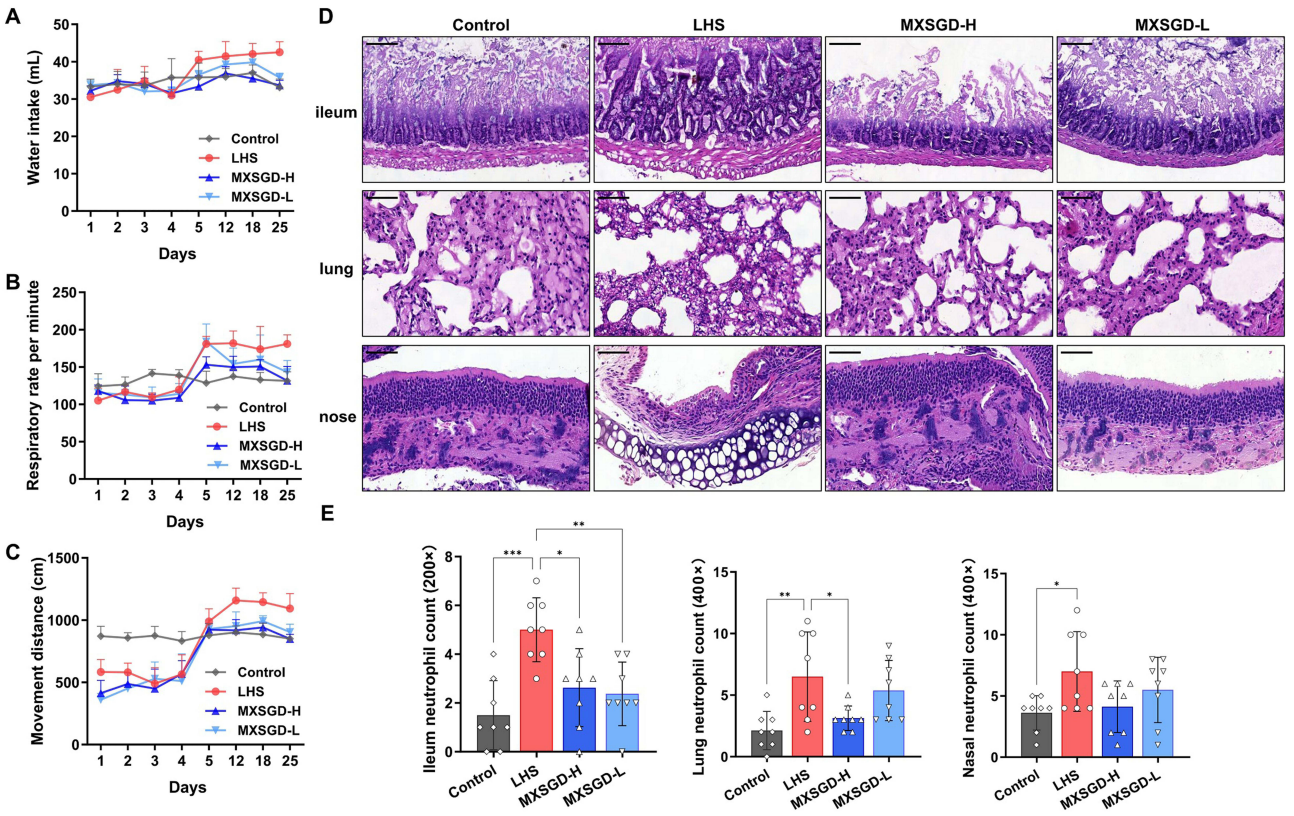

Figure 5 Effects of MXSGD on physiological and pathological parameters in LPS-challenged C57BL/6 mice. (**A**) Daily water intake (mL). (**B**) Respiratory rates. (**C**) Locomotor activity. (**D**) Representative H&E-stained sections of ileum (200×), lung (400×), and nasal mucosa (400×), scale bars = 50 μm. (**E**) Quantitative histopathological scoring of H&E findings in panel D. Data presented as mean ± SEM (n = 8/group). *$p < 0.05$, **$p < 0.01$, ***$p < 0.001$.
Abbreviations: LHS (cold stress model + lipopolysaccharide), MXSGD-H (high-dose Maxing Shigan decoction), MXSGD-L (low-dose Maxing Shigan decoction).

MXSGD ameliorated this deficit in a dose-dependent manner (Figure 5). LHS mice exhibited significant mucosal inflammation: nasal epithelium showed hyperplasia and goblet cell proliferation, lungs displayed widened alveolar septa with epithelial detachment, and ileum demonstrated structural disruption. Neutrophil infiltration increased markedly in all tissues. MXSGD-H treatment substantially attenuated these changes, reducing neutrophil counts and ameliorating epithelial hyperplasia. MXSGD-L showed intermediate efficacy, confirming dose-dependent anti-inflammatory activity (Figure 5).

MXSGD Ameliorated LHS-Induced γδT17 Cell Expansion and RORγt Overexpression Across Tissues

Further analysis evaluated the impact of LHS modeling and MXSGD treatment on γδT17 cell proportions, cytokine levels, and RORγt expression within the intestinal, pulmonary, and nasal mucosal tissues. LHS consistently resulted in a marked elevation of γδT17 cell percentages in lung and nasal mucosa compared to the Control group (Figure 6). IL-17A levels were significantly increased in the ileum and lung of LHS mice. LHS induced tissue-dependent alterations in IL-1β and IL-23, with decreased CCL25 elevation in nasal mucosa. LHS modeling also significantly upregulated the relative expression of the transcription factor RORγt in these tissues. MXSGD significantly reduced the elevated γδT17 cell proportions in pulmonary and nasal tissues. Similarly, MXSGD treatment attenuated the heightened IL-17A levels observed in the LHS ileum and lung. MXSGD also modulated IL-1β towards normalization, significantly upregulated CCL25 in nasal mucosa and downregulated LHS-induced RORγt overexpression across all tissues (Figure 6).

Effects of MXSGD on γδT17 Cell Migration and Tissue Recruitment

To investigate γδT17 cell migration patterns, we first quantified $\alpha4\beta7^{+}$γδT17 cell proportions across intestinal, pulmonary, and mucosal tissues, revealing significant LHS-associated increases in this homing receptor (Figure 7). Subsequent

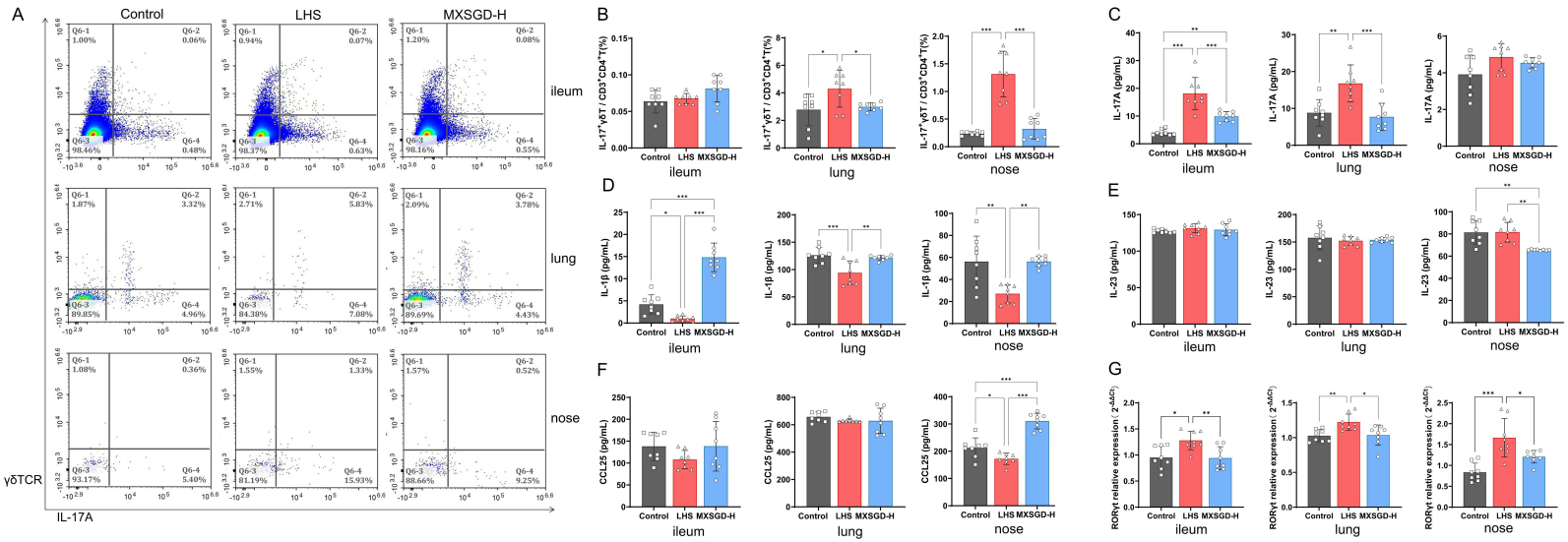

Figure 6 Effects of MXSGD on γδT17 cells, cytokine levels, and RORγt expression in tissues of LHS mice. (**A**) Representative flow cytometry plots gating on γδT17 cells in intestinal, pulmonary, and nasal mucosal tissues. (**B**) Quantitative analysis of γδT17 cell proportions. (C~F) Levels of IL-17A (C), IL-1β (D), IL-23 (E), and CCL25 (F). (**G**) Relative mRNA expression of RORγt. Data are presented as mean ± SEM (n=8/group). *$p < 0.05$, **$p < 0.01$, ***$p < 0.001$.

Abbreviations: MXSGD-H, high-dose Maxing Shigan decoction; LHS, lung heat syndrome; RORγt, retinoic acid receptor-related orphan receptor gamma t.

adoptive transfer experiments demonstrated that MXSGD treatment significantly reduced $CFSE^{+}$γδT17 cell proportions in pulmonary tissue, with a notable attenuation trend in intestinal and nasal mucosa (Figure 7). The reduced recruitment of $CFSE^{+}$ γδT17 cells in MXSGD-H treated LHS mice compared to untreated LHS mice suggests that MXSGD inhibits γδT17 cell migration to mucosal sites.

CCL25 Mediated γδT17 Cell Recruitment in MXSGD Treatment

To elucidate the role of CCL25 in MXSGD's modulation of γδT17 cell migration, we manipulated CCL25 levels in LHS-induced mice. Compared to controls, recombinant CCL25 administration significantly amplified γδT17 cell infiltration across ileum and lung tissues. In contrast, blockade of CCL25 markedly inhibited γδT17 cell recruitment in the ileum and lung tissue relative to the control group (Figure 8). Crucially, the proportion of $α4β7^{+}$γδT17 cells was significantly increased in the lung tissue of CCL25-H mice and decreased in the CCL25-L group, while no significant changes were observed in the intestine or nasal mucosa. IL-17A levels were substantially elevated in CCL25-H mice in ileum and lung tissues, but reduced in CCL25-L mice. These data demonstrate that CCL25 might be a critical mediator of α4β7-mediated γδT17 cell homing to the lung in LHS. While trends were observed, its role in the intestine and nasal mucosa under these conditions may be modulated by additional factors.

α4β7 Integrin Blockade Attenuated γδT17 Cell Recruitment and Modulated Inflammatory Responses in MXSGD's Treatment

To specifically investigate the role of α4β7 integrin in γδT17 cell migration in MXSGD's treatment, we administered anti-α4β7 antibody to LHS model mice. The blockade of α4β7 significantly reduced γδT17 cell proportions in nasal mucosa and demonstrated a decreasing trend in intestinal tissue compared to PBS-treated LHS controls. While pulmonary γδT17 cell infiltration showed moderate reduction, this did not reach statistical significance (Figure 9). α4β7 blockade markedly suppressed IL-17A production in the nasal compartment and showed a non-significant decreasing trend in the lung tissue. CCL25 quantification revealed no statistically significant alterations in its levels following α4β7 blockade in any of the tissues examined. These results demonstrated that α4β7 blockade effectively attenuated IL-17-driven inflammation in MXSGD's treatment, especially in nasal mucosa.

Discussion

This study demonstrated that MXSGD ameliorated LHS by suppressing γδT17 cell migration across the gut-lung-nasal axis via inhibition of the α4β7 integrin. Using a murine LHS model induced by wind-cold exposure and LPS challenge, we observed that MXSGD: (i) significantly reduced pathological symptoms (Figure 5); (ii) reduced γδT17 cell expansion in the lung and nose, decreased IL-17A levels in the gut and lung, and downregulated the master transcription factor RORγt across all three mucosal sites (Figure 6); (iii) inhibited α4β7-mediated γδT17 cell trafficking, as evidenced by adoptive transfer assays (Figure 7). Our results mechanistically decoded two core TCM theories: First, the "lung-intestine correlation" is substantiated by α4β7-dependent γδT17 cell migration from gut to lung/nasal tissues. Second, the TCM theory "lung opening at the nose" is validated by γδT17 infiltration in LHS (Figure 6), reflecting the decoction's capacity to clear "heat" through this orifice. MXSGD's bioactive components particularly glycyrrhizic acid and liquiritin directly bind α4β7 integrin with high affinity (Table 1, Figure 4), thereby disrupting the gut-originated "heat toxin" transmission along the mucosal axis. Our work establishes γδT17 cell migration as the missing link between TCM's meridian theory and modern immunology, positioning MXSGD as a targeted therapy that resolves systemic "heat" by compartmentalizing mucosal immunity.

The findings substantiated the TCM principle of "lung-intestine correlation" wherein lung heat pathogenesis involves interconnected mucosal barriers. MXSGD's dual-action strategy- "releasing the exterior" through immunomodulation and "clearing interior heat" via cytokine suppression aligns with its documented anti-inflammatory effects.[8,28] The α4β7 integrin emerge as a biochemical correlate to the TCM meridians governing lung-intestine communication, as γδT17 cell trafficking mirrors the pathological transmission of "heat toxin" from the gut to the lung.

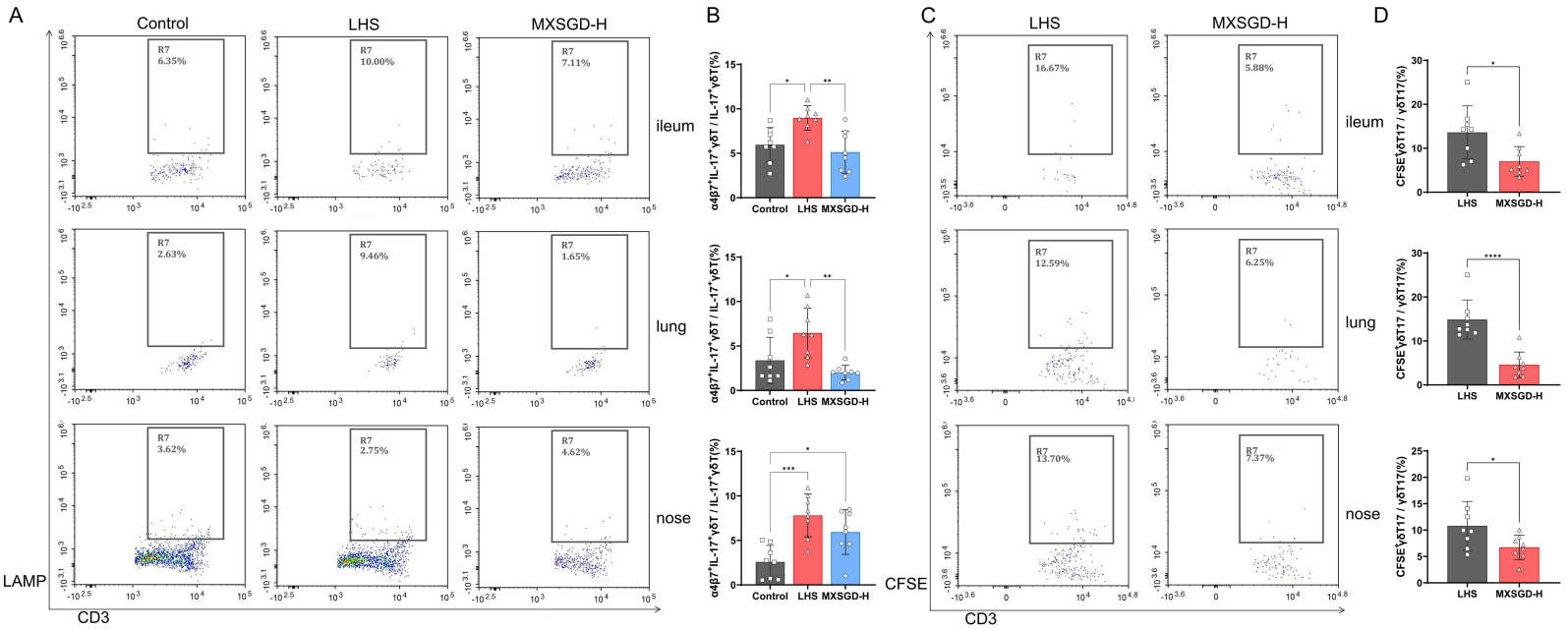

Figure 7 MXSGD inhibited γδT17 cell recruitment to mucosal tissues. (**A**) Representative flow cytometry plots showing $\alpha4\beta7^+\gamma\delta$T17 cells in intestinal, pulmonary, and mucosal tissues. (**B**) Quantitative analysis of $\alpha4\beta7^+\gamma\delta$T17 cells across groups. (**C**) Representative flow cytometry plots showing $CFSE^+\gamma\delta$T17 cells in intestinal, pulmonary, and mucosal tissues. (**D**) Quantitative analysis of $CFSE^+\gamma\delta$T17 cells across groups. (n=8/group). Data are presented as mean ± SEM (n=8/group). *$p < 0.05$, **$p < 0.01$, ***$p < 0.001$, ****$p < 0.0001$.

Abbreviations: MXSGD-H, high-dose Maxing Shigan Decoction; CFSE, carboxyfluorescein succinimidyl ester.

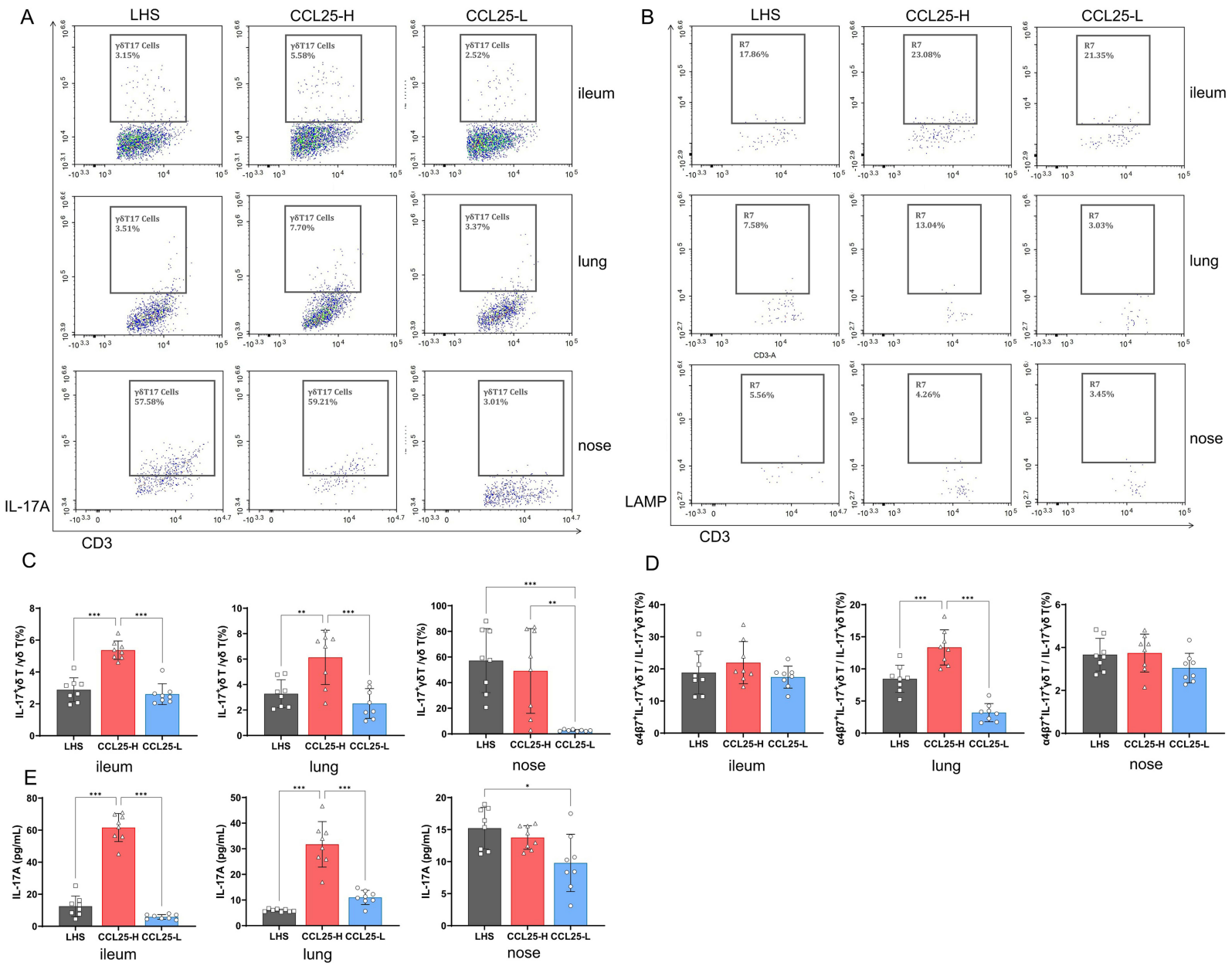

Figure 8 CCL25-dependent regulation of γδT17 cell recruitment and IL-17 production. (**A**) Representative flow cytometry plots showing γδT17 cell populations in intestinal, pulmonary, and nasal mucosal tissues. (**B**) Representative flow cytometry plots showing $\alpha4\beta7^+$γδT17 cells. (**C**) Quantitative analysis of γδT17 cell proportions. (**D**) Quantitative analysis of $\alpha4\beta7^+$γδT17 cells proportions. (**E**) IL-17A levels. Data represent mean ± SEM (n=8/group). *$p < 0.05$, **$p < 0.01$, ***$p < 0.001$.
Abbreviations: CCL25-H, high CCL25 group; CCL25-L, CCL25-neutralized group.

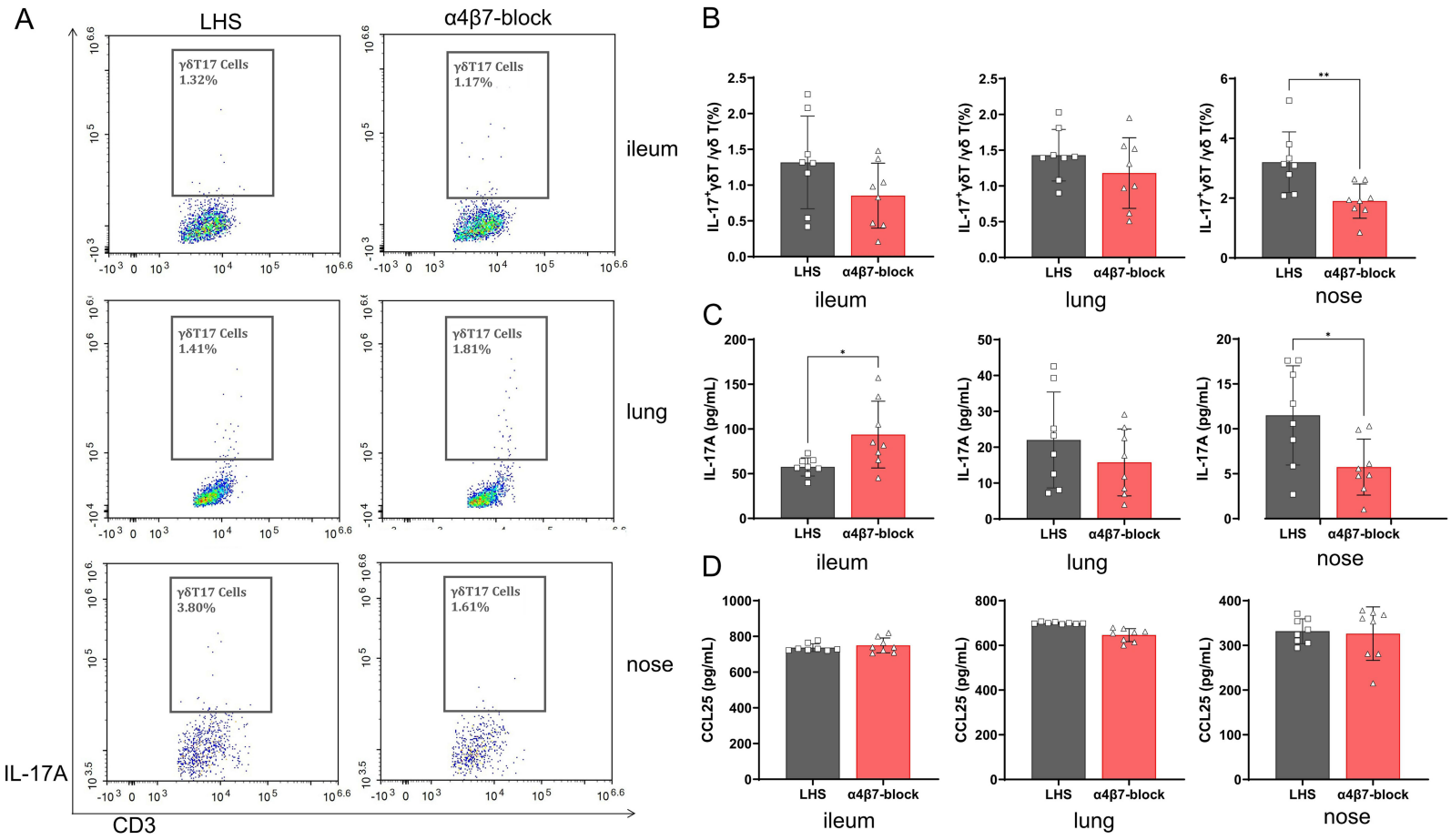

Figure 9 α4β7 integrin blockade attenuated γδT17 cell recruitment and modulated mucosal inflammation. (**A**) Representative flow cytometry plots of γδT17 cells in intestinal, pulmonary, and nasal mucosa. (**B**) Quantitative analysis of γδT17 cell proportions (**C**) IL-17A levels. (**D**) CCL25 levels. Data represent mean ± SEM (n=8/group). *$p < 0.05$, **$p < 0.01$.
Abbreviation: LHS, lung heat syndrome.

A key finding that clarifies MXSGD's mechanism is the dissociation between CCL25 levels and γδT17 cell recruitment. Specifically, MXSGD-H treatment was associated with elevated nasal CCL25 yet a significant reduction in γδT17 cells (Figure 6). This indicates that the decoction does not exert its effect by quenching the chemotactic signal. While CCL25 is classically associated with intestinal homing via CCR9,[29,30] its pronounced elevation in nasal mucosa (Figure 6) revealed tissue-agnostic chemotactic properties. Crucially, molecular docking identified liquiritin (ΔG = −13.7 kcal/mol) and glycyrrhizic acid (ΔG = −11.5 kcal/mol) as high-affinity MXSGD ligands for α4β7 integrin (Table 1), and functional blockade of α4β7 recapitulated the anti-migratory effects of MXSGD (Figure 9). Thus, we propose that MXSGD acts as a functional antagonist of α4β7, effectively "disarming" γδT17 cells and preventing their response to CCL25, regardless of the chemokine's concentration.

The distinct biological properties of γδT17 cells render them particularly relevant to the pathogenesis of LHS and the rapid therapeutic efficacy observed with MXSGD (Figure 5). Unlike conventional Th17 cells, γδT17 cells are primarily tissue-resident, particularly abundant in mucosal barriers like the gut, and poised for rapid, antigen-independent activation.[17,18,31] This intrinsic capacity for swift IL-17A secretion aligns perfectly with the acute onset and rapid progression of LHS symptoms induced by our wind-cold/LPS model. In contrast, Th17 cells, while potent IL-17 producers, require antigen presentation, clonal expansion in lymphoid organs, and subsequent homing, processes typically taking 3–5 days to mount a significant effector response.[32] The rapid suppression of γδT17 cell migration and IL-17A production across mucosal tissues within days of MXSGD intervention, coinciding with the swift alleviation of pathological symptoms, strongly supports the targeting of this fast-reacting γδT17 axis as the cornerstone of MXSGD's prompt efficacy against the "heat syndrome". Our findings extended current gut-lung axis models[33,34] by identifying γδT17 instead of Th17 as the dominant migratory effector in LHS.

While the study elucidated mechanisms of MXSGD action, several limitations warrant consideration, including the need for lineage tracing to definitively confirm gut-derived γδT17 cells in nasal mucosa and clinical validation in human LHS patients. Future investigations should employ single-cell RNA sequencing to characterize γδT17 heterogeneity across mucosal tissues and explore the pharmacokinetic optimization of MXSGD's active components. Additionally, employing Western blot analysis would be valuable to confirm the findings at the protein level and to further elucidate the involvement of upstream signaling pathways, such as STAT3 phosphorylation.

Conclusion

This work provided transformative insights into the immunomodulatory mechanisms of MXSGD by demonstrating its inhibition of α4β7-mediated γδT17 cell trafficking and IL-17A production across the gut-lung-nasal axis. Our findings not only validated the scientific basis of TCM's lung-intestine correlation theory but also identified specific bioactive compounds as natural inhibitors of α4β7 integrin. We established a new paradigm for developing targeted ethnopharmacological interventions against mucosal inflammation, offering mechanistic clarity and translational potential for MXSGD.

Abbreviations

LHS, Lung Heat Syndrome; MXSGD, Maxing Shigan decoction; IL-17A, Interleukin-17A; TCM, Traditional Chinese medicine; Th17, T helper 17 cell; CCL25, C-C motif chemokine ligand 25; UPLC-Q-ToF-HRMS, Ultra-performance liquid chromatography quadrupole-time-of-flight high-resolution mass spectrometry; TCMSP, Traditional Chinese medicine systems pharmacology; PPI, Protein- protein interaction; GO, gene ontology; KEGG, Kyoto encyclopedia of genes and genomes; H&E, Hematoxylin and eosin; ELISA, Enzyme-linked immunosorbent assay; RT-PCR, Reverse transcription-polymerase chain reaction; RORγt, Retinoic acid receptor-related orphan receptor gamma t; CFSE, Carboxyfluorescein succinimidyl ester; rmCCL25, Recombinant mouse CCL25; MCODE, Molecular complex detection.

Data Sharing Statement

The original contributions presented in the study are included in the article and Supplementary Material, further inquiries can be directed to the corresponding author.

Ethics Statement

All procedures were approved by the Institutional Animal Care and Use Committee of the Beijing Hospital of Traditional Chinese Medicine (No. SQ-2022-02-35, granted in February 2022), and strictly adhered to the use and care of laboratory animals outlined by the People's Republic of China's legislation and the National Research Council's Guide.

Author Contributions

All authors made a significant contribution to the work reported, whether that is in the conception, study design, execution, acquisition of data, analysis and interpretation, or in all these areas; took part in drafting, revising or critically reviewing the article; gave final approval of the version to be published; have agreed on the journal to which the article has been submitted; and agree to be accountable for all aspects of the work.

Funding

This work was supported by the National Natural Science Foundation of China [grant number 82205203].

Disclosure

The authors declared no conflicts of interest in this work.

References

1. Yang J, Yang J. Clearing heat and resolving phlegm for acute exacerbation of chronic obstructive pulmonary disease with the syndrome of phlegm-heat obstruction of the lung. *J Int Med Res*. 2020;48(8):300060520945502. doi:10.1177/0300060520945502
2. Chen J, Zhu Z, Gao T, et al. Isatidis Radix and Isatidis Folium: a systematic review on ethnopharmacology, phytochemistry and pharmacology. *J Ethnopharmacol*. 2022;283:114648. doi:10.1016/j.jep.2021.114648
3. Zhang F, Ke C, Zhou Z, et al. Scutellaria baicalensis pith-decayed root inhibits macrophage-related inflammation through the NF-κB/NLRP3 pathway to alleviate LPS-induced acute lung injury. *Planta Med*. 2023;89(5):493–507. doi:10.1055/a-1878-5704
4. Xia C, Lin L, Zhang H. Effects of yupingfeng granules combined with pediatric lung heat cough asthma on serum inflammatory factors and T lymphocyte subsets in children with Mycoplasma pneumonia. *Minerva Pediatr*. 2024. doi:10.23736/S2724-5276.24.07686-9
5. Chen P, Lin C, Jin Q, et al. Investigating mechanisms of Sophora davidii (Franch.) skeels flower extract in treating LPS-induced acute pneumonia based on network pharmacology. *J Ethnopharmacol*. 2025;337(Pt 2):118914. doi:10.1016/j.jep.2024.118914
6. Li Y, Chu F, Li P, et al. Potential effect of Maxing Shigan decoction against coronavirus disease 2019 (COVID-19) revealed by network pharmacology and experimental verification. *J Ethnopharmacol*. 2021;271:113854. doi:10.1016/j.jep.2021.113854
7. Cheng M, Zhang Y, Yan J, et al. Inhibiting virus replication and excessive inflammatory response: mechanism of combined prescription of Ma-Xing-Shi-Gan decoction and Xiao-Chai-Hu decoction against influenza virus. *J Ethnopharmacol*. 2023;313:116481. doi:10.1016/j.jep.2023.116481
8. Huang J, Ma X, Liao Z, et al. Network pharmacology and experimental validation of Maxing Shigan decoction in the treatment of influenza virus-induced ferroptosis. *Chin J Nat Med*. 2023;21(10):775–788. doi:10.1016/S1875-5364(23)60457-1
9. Xu Y, Bao L, Cao S, et al. Pharmacological effects and mechanism of Maxing Shigan decoction in the treatment of Pseudomonas aeruginosa pneumonia. *J Ethnopharmacol*. 2024;320:117424. doi:10.1016/j.jep.2023.117424
10. Zhang S, Li B, Zeng L, et al. Exploring the immune-inflammatory mechanism of Maxing Shigan Decoction in treating influenza virus A-induced pneumonia based on an integrated strategy of single-cell transcriptomics and systems biology. *Eur J Med Res*. 2024;29(1):234. doi:10.1186/s40001-024-01777-9
11. Jiao J, Tang Q, Wang TJ, et al. The therapeutic effect of Xuanbai Chengqi Decoction on chronic obstructive pulmonary disease with excessive heat in the lung and fu-organs based on gut and lung microbiota as well as metabolic profiles. *J Chromatogr B Analyt Technol Biomed Life Sci*. 2022;1198:123250. doi:10.1016/j.jchromb.2022.123250
12. Niu Q, Lu Y, Ren M, et al. Alterations of lung and gut microbiota in sodium butyrate alleviating heat stress-induced lung injury of broilers. *Poult Sci*. 2025;104(2):104796. doi:10.1016/j.psj.2025.104796
13. Sayedahmed EE, Elshafie NO, Zhang G, Mohammed SI, Sambhara S, Mittal SK. Enhancement of mucosal innate and adaptive immunity following intranasal immunization of mice with a bovine adenoviral vector. *Front Immunol*. 2023;14:1305937. doi:10.3389/fimmu.2023.1305937
14. Lian YB, Hu MJ, Guo TK, et al. The protective effect of intranasal immunization with influenza virus recombinant adenovirus vaccine on mucosal and systemic immune response. *Int Immunopharmacol*. 2024;130:111710. doi:10.1016/j.intimp.2024.111710
15. Wang X, Zhang K, Zhang J, et al. Cordyceps militaris solid medium extract alleviates lipopolysaccharide-induced acute lung injury via regulating gut microbiota and metabolism. *Front Immunol*. 2024;15:1528222. doi:10.3389/fimmu.2024.1528222
16. Ziaka M, Exadaktylos A. Gut-derived immune cells and the gut-lung axis in ARDS. *Crit Care*. 2024;28(1):220. doi:10.1186/s13054-024-05006-x
17. Khairallah C, Chu TH, Sheridan BS. Tissue adaptations of memory and tissue-resident Gamma Delta T Cells. *Front Immunol*. 2018;9:2636. doi:10.3389/fimmu.2018.02636
18. Li GQ, Xia J, Zeng W, et al. The intestinal γδ T cells: functions in the gut and in the distant organs. *Front Immunol*. 2023;14:1206299. doi:10.3389/fimmu.2023.1206299
19. Xie B, Wang M, Zhang X, et al. Gut-derived memory γδ T17 cells exacerbate sepsis-induced acute lung injury in mice. *Nat Commun*. 2024;15(1):6737. doi:10.1038/s41467-024-51209-9

20. Fu H, Jangani M, Parmar A, et al. A subset of CCL25-induced gut-homing T cells affects intestinal immunity to infection and cancer. *Front Immunol*. 2019;10:271. doi:10.3389/fimmu.2019.00271
21. Zhang Y, Han J, Wu M, et al. Toll-like receptor 4 promotes Th17 lymphocyte infiltration via CCL25/CCR9 in pathogenesis of experimental autoimmune encephalomyelitis. *J Neuroimmune Pharmacol*. 2019;14(3):493–502. doi:10.1007/s11481-019-09854-1
22. Wyant T, Fedyk E, Abhyankar B. An overview of the mechanism of action of the monoclonal antibody vedolizumab. *J Crohns Colitis*. 2016;10 (12):1437–1444. doi:10.1093/ecco-jcc/jjw092
23. Costa MF, Bornstein VU, Candéa AL, Henriques-Pons A, Henriques MG, Penido C. CCL25 induces $\alpha_4\beta_7$ integrin-dependent migration of IL-17207A$^+$ γδ T lymphocytes during an allergic reaction. *Eur J Immunol*. 2012;42(5):1250–1260. doi:10.1002/eji.201142021
24. Do JS, Kim S, Keslar K, et al. γδ T cells coexpressing gut homing α4β7 and αE integrins define a novel subset promoting intestinal inflammation. *J Immunol*. 2017;198(2):908–915. doi:10.4049/jimmunol.1601060
25. Bardou P, Mariette J, Escudié F, Djemiel C, Klopp C. jvenn: an interactive Venn diagram viewer. *BMC Bioinf*. 2014;15(1):293. doi:10.1186/1471-2105-15-293
26. Tang D, Chen M, Huang X, et al. SRplot: a free online platform for data visualization and graphing. *PLoS One*. 2023;18(11):e0294236. doi:10.1371/journal.pone.0294236
27. Yang R, Liu H, Bai C, et al. Chemical composition and pharmacological mechanism of Qingfei Paidu decoction and Ma Xing Shi Gan decoction against Coronavirus Disease 2019 (COVID-19): in silico and experimental study. *Pharmacol Res*. 2020;157:104820. doi:10.1016/j.phrs.2020.104820
28. Huang H, Yang H, Zhang Z, et al. Synergistic therapeutic effects and immunoregulatory mechanism of Maxing Shigan decoction combined with Sijunzi Decoction on viral Pneumonia in mice. *Can J Infect Dis Med Microbiol*. 2024;2024:2017992. doi:10.1155/2024/2017992
29. Trivedi PJ, Bruns T, Ward S, et al. Intestinal CCL25 expression is increased in colitis and correlates with inflammatory activity. *J Autoimmun*. 2016;68:98–104. doi:10.1016/j.jaut.2016.01.001
30. Aghaallaei N, Agarwal R, Benjaminsen J, et al. Antigen-presenting cells and T cells interact in a specific area of the intestinal Mucosa defined by the Ccl25-Ccr9 Axis in Medaka. *Front Immunol*. 2022;13:812899. doi:10.3389/fimmu.2022.812899
31. Papotto PH, Ribot JC, Silva-Santos B. IL-17(+) γδ T cells as kick-starters of inflammation. *Nat Immunol*. 2017;18(6):604–611. doi:10.1038/ni.3726
32. Gupta PK, Wagner SR, Wu Q, Shilling RA. Th17 cells are not required for maintenance of IL-17A-producing γδ T cells in vivo. *Immunol Cell Biol*. 2017;95(3):280–286. doi:10.1038/icb.2016.94
33. Hong Y, Chu Z, Kong J, et al. IL-17A aggravates asthma-induced intestinal immune injury by promoting neutrophil trafficking. *J Leukoc Biol*. 2022;112(3):425–435. doi:10.1002/JLB.3MA0622-426RR
34. Shi C, Zhou L, Li H, et al. Intestinal microbiota metabolizing Houttuynia cordata polysaccharides in H1N1 induced pneumonia mice contributed to Th17/Treg rebalance in gut-lung axis. *Int J Biol Macromol*. 2022;221:288–302. doi:10.1016/j.ijbiomac.2022.09.015